metals

MDPI

Article

Microstructural Evolution in a 0.09% Niobium Low Carbon Steel during Controlled Hot Deformation

E. Pineda Martínez and E. J. Palmiere *

Department of Materials Science and Engineering, The University of Sheffield, Sir Robert Hadfield Building, Mappin Street, Sheffield S1 3JD, UK

* Correspondence: e.j.palmiere@sheffield.ac.uk; Tel.: +44-(0)-114-222-5978

Abstract: A series of plane strain compression tests were carried out in order to simulate the thermo-mechanical controlled processing of a 0.09wt% Nb low carbon steel, in a scheme of multipass finish rolling at 950 °C with interpass times of 10 s. It was observed that after the first two finishing passes a remarkable grain refinement can be achieved, since the recrystallisation was fully suppressed and abundant ultrafine ferrite was transformed dynamically during the deformation. The addition of a third finishing pass however, led to partial recrystallisation. A deep characterisation of the dynamic ferrite was carried out by diverse methods conducting to relevant findings that contribute to a better elucidation of the dynamic transformation. The results obtained indicated that the dynamic formation of a colony of Widmanstätten ferrite plates during deformation, initiates with the formation of a pair of self-accommodating plates followed by face-to-face sympathetic nucleation of new plates at one of the faces of the pairs of plates already formed. Furthermore, the crystal orientation within the dynamic ferrite phase was analysed with EBSD, it was observed that during the coalescence of plates, prior to the full polygonisation of grains, the ferrite adopts a transitory morphology which possesses particular crystallographic characteristics.

Keywords: ultrafine steel; dynamic ferrite transformation; microstructural evolution; thermomechanical controlled processing (TMCP)

Citation: Martínez, E.P.; Palmiere, E.J. Microstructural Evolution in a 0.09% Niobium Low Carbon Steel during Controlled Hot Deformation. *Metals* **2024**, *14*, 283. https://doi.org/10.3390/met14030283

Academic Editors: Atef Saad Hamada, Koh-ichi Sugimoto, José Valdemar Fernandes and Tomohiko Hojo

Received: 8 January 2024
Revised: 20 February 2024
Accepted: 26 February 2024
Published: 28 February 2024

1. Introduction

Within the last five decades, extensive research has been focused to improve the ferrite grain size refinement, the increasing demand of structural steels with higher strength and toughness has produced a global trend towards the research and development of steels with microstructures as fine as possible. The austenite to ferrite dynamic transformation during deformation seems to be a promising alternative to produce ultrafine grained microstructures, a proper combination of deformation variables and alloy design can lead to microstructures with a grain size on the order of 1 μm or even smaller.

The first observations of the dynamic transformation were reported in the patent registered in the 1980s [1], who performed large deformations in common C-Mn steels at approximately the Ar_3 temperature and then rapidly quenched, the final microstructure consisted of 70% or more of equiaxed ferrite grains with a size of 4 μm or less. In later works [2–8], the dynamic transformation was also observed at temperatures above the Ae_3 in plain carbon steels, the combination of large strains and multiple passes conducted to ultrafine grains of ferrite of around 2 μm. Extensive research has been carried out after the pioneering work of Yada and co-workers and numerous papers have been published mainly in the last two decades.

One of the most polemic topics has been the transformation mechanism of the dynamic ferrite, at least four different approaches [4–15] can be found in the literature attempting to explain the transformation path. One of the most accepted interpretations of the transformation mechanisms was proposed by [16], who carried out torsion tests above the Ae_3

temperature at strains from 0.5 to 2 in a steel containing 0.09%C-1.3%Mn-0.02%Si-0.036%Nb. According to their findings, the deformation causes the displacive transformation of thin Widmanstätten ferrite plates of about 200 nm wide that subsequently merge by coalescence and evolve into polygonal grains. Ferrite plates appear aligned in a single direction showing the influence of the stress during the deformation, and the nucleation can occur at the prior austenite grain boundaries in addition to intragranular. EBSD analysis showed that the angular misorientation between adjacent plates is very small (less than or around 1°), which accounts for the rapid coalescence of plates that leads to polygonal grain formation. Basabe et al. used the term "dynamic transformation" (DT) to refer to the ferrite formed during deformation at temperatures above the Ae_3.

The DT has received increased attention and numerous works [17–21] have been published supporting this hypothesis over the recent years, and the transformation mechanism has been one of subjects of major interest. For example, Jonas & Ghosh [22] developed a model to describe the DT of the Widmanstätten ferrite plates. According to their work, the transformation occurs by mechanical activation conducting to the formation of pairs of self-accommodating plates of near-identical orientation [23]. The stress provides the energy required to accommodate the shear of the parent austenite into Widmanstätten plates as well as the volume change or dilatation needed for the ferrite formation. The application of a shear stress conducts to the formation of a ferrite plate that forces the adjacent austenite to shear along with one of the sides of the plate, then the strained austenite transforms into a second ferrite plate, forming a pair of self-accommodating plates with opposite shears that cancel each other out.

2. Experimental Procedure

2.1. Material

Sections of a finished X80 pipe (from the West-East II China high pressure pipeline) with a wall thickness of 12 mm were provided by Companhia Brasileira de Metalurgia e Mineração (CBMM), Brazil. The material analysed is a High Temperature Processing (HTP) concept steel and the chemical composition is shown in Table 1.

Table 1. Chemical composition (wt%) of the HTP concept linepipe steel.

C	Mn	Si	S	P	Nb	Ti	N
0.045	1.43	0.14	0.003	0.01	0.09	0.01	0.004

2.2. Thermomechanical Processing

Before the preparation of specimen for the deformation tests, the steel sections underwent an austenitising heat treatment at 1300 °C with a holding time of 2 h and then were rapidly quenched in cold water, this treatment was done in order to fully dissolve the niobium precipitates in the steel alloy. Plane strain compression (PSC) specimens with standard dimensions (10 mm thick × 30 mm wide × 60 mm long) were machined from the sections of the steel pipe. Then, a series of PSC tests were performed in a servo-hydraulic Thermomechanical Compression (TMC) machine manufactured by Servotest Testing Systems, Ltd., Surrey, UK, in accordance to the Good Practice Guide for Hot (isothermal) Plane Strain Compression Testing [24]. The TMC machine provides a high degree of precision in the control of temperature, strain, heating/cooling rate and strain rate. PSC specimens were heated to 1200 °C at a rate of 10 °C/s, held for 2 min for equilibration, and then cooled at a rate of 10 °C/s to 1100 °C to perform a single pass roughing deformation at a strain of 0.3 and a constant true strain rate of 10 s^{-1}. After roughing, the specimens were cooled at a rate of 10 °C/s to 950 °C to perform three finishing passes at a strain of 0.22 for each pass followed by isothermal holding times of 10 s. After each deformation pass or holding time, the specimens were rapidly quenched in water within 0.5 s to analyse the microstructure at each stage of the deformation schedule.

In order to estimate the fractional softening obtained during the holding times in the finish rolling, a "monotonic finishing" test was performed and the resulting flow curved served as a reference for the TMC simulation. In this test, the rough deformation was conducted as described above but the finishing deformation consisted of a single pass at a strain ε_5 = 0.66 at 950 °C. Note that the only difference between the monotonic finishing test and the TMCP simulation is the way in which the finishing deformation is performed, in the former the specimen is strained to 0.66 in a single pass, whereas the in latter, the same amount of the deformation is applied to the specimen but divided in three finishing passes at 0.22 of strain each. A schematic representation of the thermomechanical schedules is presented in Figure 1.

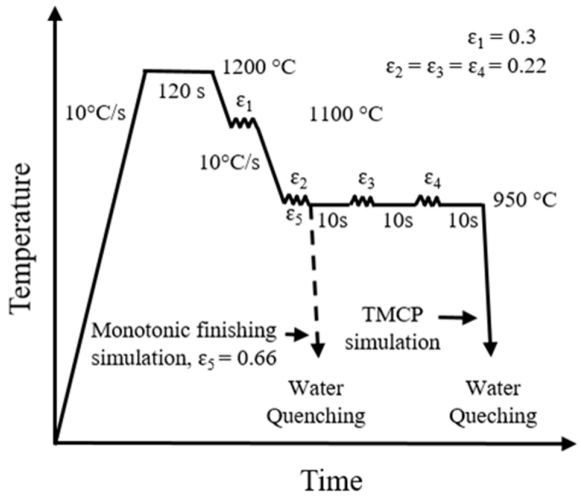

Figure 1. Thermomechanical schedule designed for the PSC tests performed at a strain rate of 10 s^{-1}.

2.3. Metallographic Evaluation

The deformed PSC specimens were sectioned in the plane of observation (rolling direction (RD) × normal direction (ND)) and mounted in conductive Bakelite for automatic preparation in a grinder-polisher machine. The surface of interest was prepared until a mirror-like finish was achieved, the final polishing was carried out using a monocrystalline diamond suspension of 1 µm. Then, the microstructure of the material was revealed using traditional metallographic methods. Microstructures were observed with optical microscopy (OM) and secondary electrons in SEM using a FEI Inspect F50 instrument at a voltage of 20 kV. To prepare the specimens for the EBSD analysis, after the sample preparation aforementioned, additional polishing from 15 to 30 min with 0.06 µm colloidal silica was done in order to improve surface quality, the colloidal silica absorbed on the polished surface was removed with an ultrasonic cleaning for at least 30 min. The analysis was conducted in the FEI Inspect F50 microscope using a voltage of 20 kV and a step size of 0.1 µm. For the observation of the prior austenite grain boundaries (PAGBs), polished samples prepared following on from other published research [25–27], and were etched between 1 and 3 min in a saturated aqueous picric acid solution at 80 °C until PAGBs were revealed, the solution was prepared with 100 mL of distilled water, 1.5 g of Sodium dodecyl sulphate as a surfactant and 5 to 7 drops of HCl. The average grain size and recrystallisation fraction were estimated for each deformation condition using at least 3 OM images, the average grain size was obtained with the linear intercept method (ASTM E-112) whereas the recrystallised fraction was determined with the point counting method. The individual steel phases were also observed in TEM; thin foils were prepared in a TenuPol-5 twin-jet automatic electropolisher using an electrolytic solution that contained 5% perchloric acid, 35% butoxyethanol and 60% methanol at −40 °C and a voltage from 30 to 32 mA. The thin foils were observed in Bright Field mode on a JEOL JEM-200 operated at a voltage of 200 kV.

3. Results

3.1. Characterisation of the Microstructure Prior to Deformation

An initial characterisation of the micro-structure after the austenitising heat treatment at 1300 °C was performed so as to observe the phases transformed during the quenching of the undeformed material. The microstructure exhibited a dominant martensitic phase (α') with some small bainitic (α_B) regions as shown in the OM image of Figure 2a. The martensite appears in form of laths with high dislocation density (see Figure 2b) as result of the rapid transformation occurred during quenching. Note that neither Widmanstätten ferrite plates nor ferrite grains are observed, which confirms that such transformation products cannot be formed in the HTP steel when undeformed austenite is water quenched. The EBSD Euler map and the grains misorientation distribution displayed in Figures 2c and 2d respectively shows a highly misoriented lath structure constituted by only low angle boundaries (<15°) and high angle boundaries in the range from 50 to 63°, which is typically observed in martensitic and/or bainitic microstructures in steel [28,29].

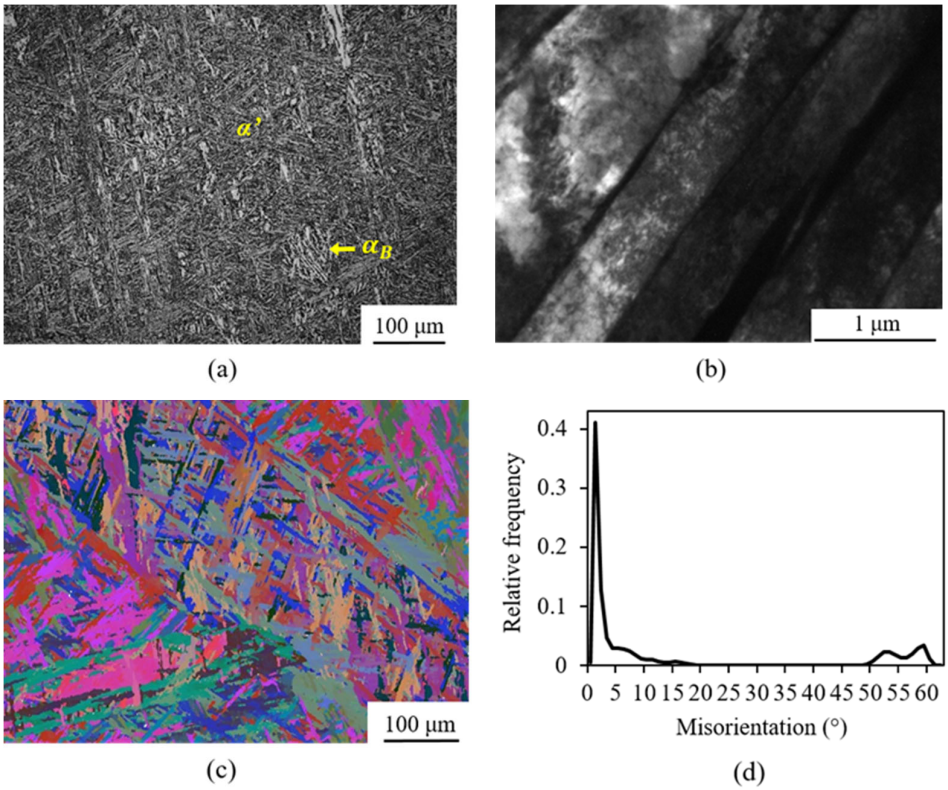

Figure 2. Characterisation of undeformed quenched specimens after the austenitising heat treatment. Martensitic dominant microstructure observed in (**a**) optical microscopy, (**b**) TEM bright field and (**c**) EBSD Euler map with its respective (**d**) grain misorientation distribution histogram.

3.2. Flow Curves

The complete flow curve showing the roughing and finishing deformations is illustrated in Figure 3, for which there is an expected increase in the stress during the finishing passes due to the accumulation of strain with decreasing deformation temperatures. It is important to highlight the drop in the initial flow stress in the second and mostly the third finishing pass, this behaviour in the flow curves indicates that important restoration took place in the microstructure during the holding time between the finishing passes.

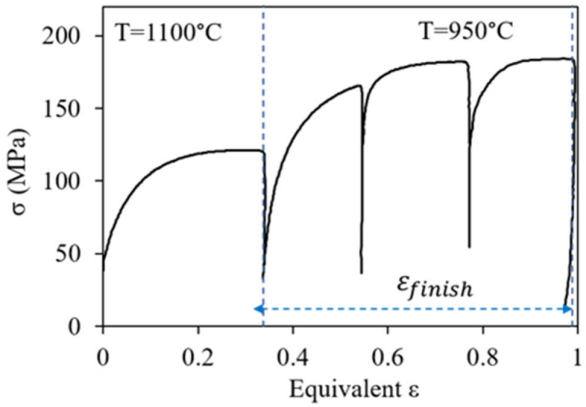

Figure 3. True stress versus equivalent strain showing the roughing and finishing passes using the thermomechanical schedule of Figure 1.

The amount of softening obtained in the second and third finishing passes was estimated using the parameter X_A, where this softening parameter was developed by Kwon and DeArdo [30] and subsequently used by Romano-Acosta et al. [31] to calculate the fractional softening from the area under the flow curves and is expressed as below:

$$X_A = \frac{A_3 - A_2}{A_3 - A_1} \quad (1)$$

where A_1 and A_2 are the areas under the flow stress curve of the first and second deformation in the interrupted test respectively, and A_3 is the area under the flow curve in the monotonic test over the strained region equivalent to the second deformation in the interrupted tests.

The segment of the flow curve containing the three finishing passes (ε_{finish} of Figure 3) was used as the interrupted test and plotted together with the finishing pass at 950 °C of the monotonic test, then the Equation (1) was used to estimate the fractional softening obtained after the interpass times in the finish rolling simulation as illustrated in Figure 4a,b.

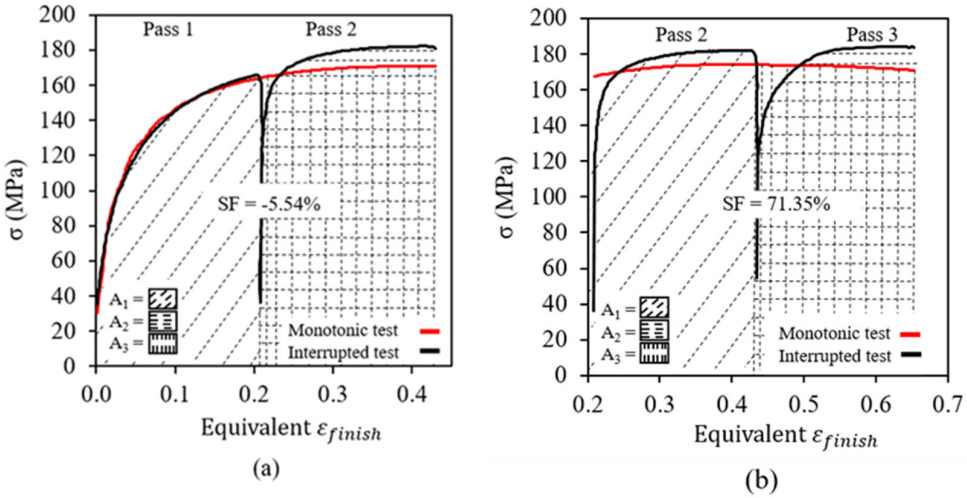

Figure 4. Flow curves used to estimate the softening fraction (SF = X_A − 100%) obtained after (**a**) the first and (**b**) second interpass time.

In the second finishing pass the material experienced a subtle hardening of around 6%, whereas in the third pass the behaviour changed drastically since the softening obtained was 71%. The low hardening obtained in the second finishing pass and the significant softening in the third one, are associated with the transformation and evolution of dynamic

ferrite. During deformation, the dynamic transformation causes lower than expected stress levels in the flow curves since ferrite is softer than austenite [32,33]. Then during the holding time, although the dynamic transformation cannot occur, the evolution of Widmanstätten ferrite plates into polygonal grains can provide great softening to the microstructure. Evidence of this, can be clearly observed in the second holding time in which the fractional softening was remarkable despite the static recrystallisation of PAGs was negligible (the analysis of recrystallisation is presented in the following section).

3.3. Morphology of the Prior Austenite Grain Boundaries (PAGBs)

The evolution of the PAGBs in each condition of the simulation is shown in Figure 5 and the measurements of the grain size and recrystallised fraction measured using point count stereology are presented in Table 2. Prior to deformation, the prior austenite grains were very coarse and polygonal with an average size of 87 μm. Microstructural refinement was observed following the single roughing pass at 1100 °C which led to a fully recrystallised microstructure with an average grain size of 25 μm. In the following two finishing passes, the austenite was successively deformed and the grains adopted a shape elongated along the rolling direction (RD), the recrystallisation fraction after the first and second finishing passes were 11.6% and 1.2% respectively. Note that the static recrystallisation during the holding time after these passes was negligible, which indicates that the insipient dynamic recrystallisation was effectively suppressed during or immediately after the deformation enhancing the microstructural refinement. The addition of the third finishing pass, however, increased the recrystallised fraction to 20% which is inconvenient for the microstructural refinement since coarser prior austenite grains lead to the transformation of coarser microstructures on cooling. The PAGBs after the third holding time could not be clearly revealed with aqueous picric acid solution after multiple attempts, thus the average grain size could not be estimated with accuracy and it is not reported.

Table 2. Prior austenite grain size and recrystallised fraction measured in each condition.

Quenched Specimen Obtained Immediately after:	Recrystallised Fraction (%)	Average Grain Diameter (μm)		Aspect Ratio
		Rolling Direction	Normal Direction	
Austenitising heat treatment	-	88.4	83.4	1.06
Roughing pass	100	25.1	24.8	1.01
First finishing pass	11.7	48.2	20.3	2.37
First holding time	12.6	46.5	18.1	2.57
Second finishing pass	1.2	70.4	12.4	5.68
Second holding time	1.3	68.4	11.3	6.05
Third holding time	20	-	-	-

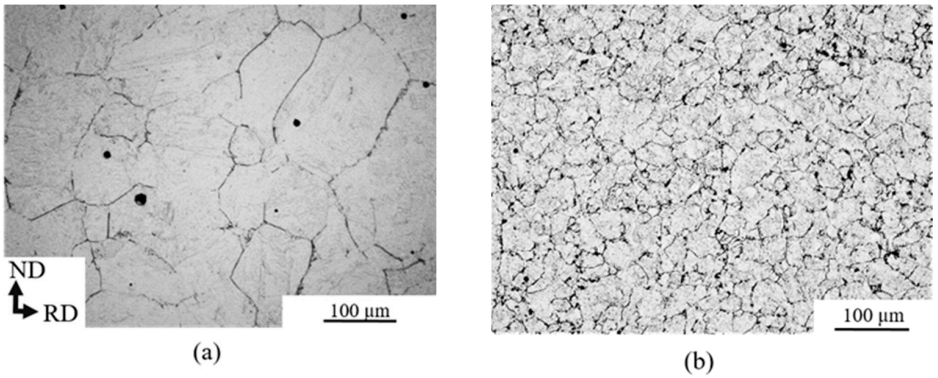

Figure 5. *Cont.*

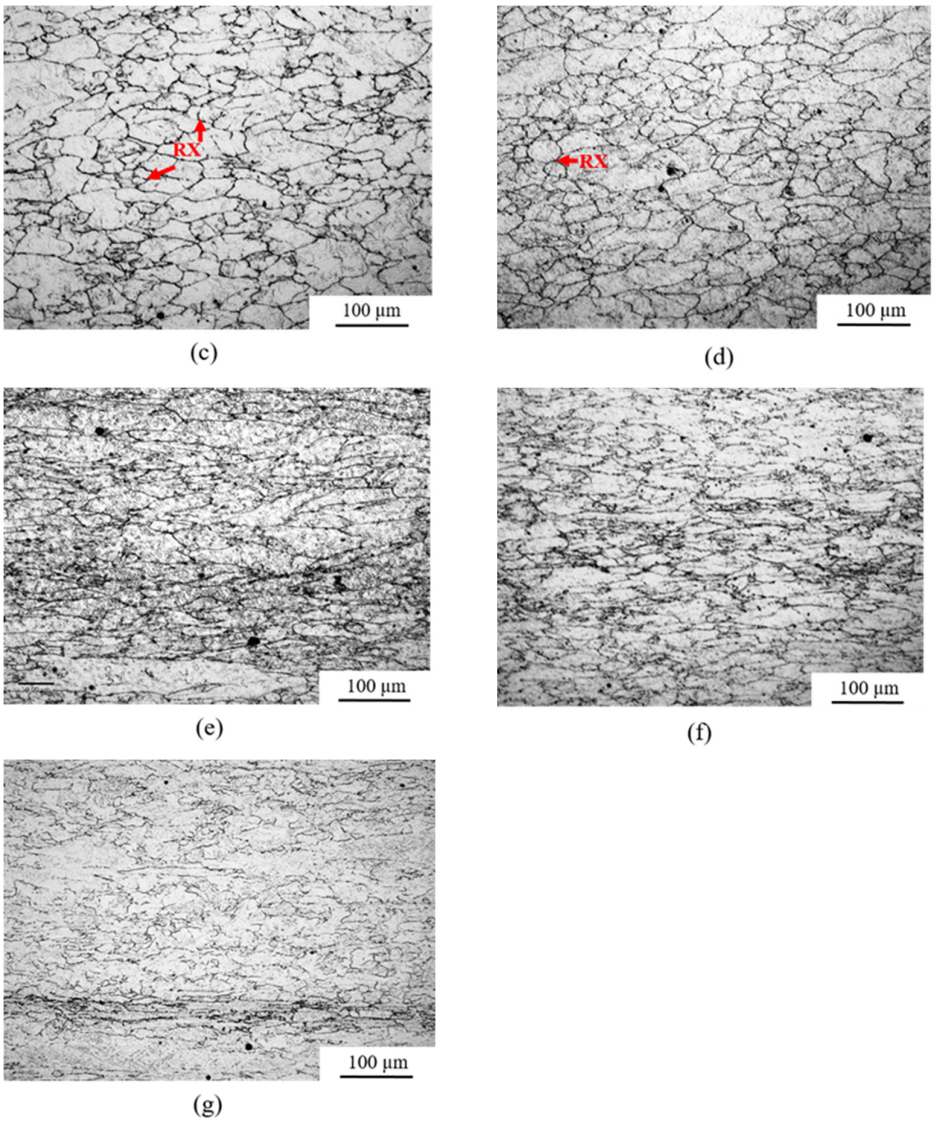

Figure 5. Prior austenite grain boundaries revealed in quenched samples after; (**a**) the austenitising heat treatment, (**b**) the roughing pass, (**c**) one finishing pass, (**d**) the first holding time, (**e**) 2 finishing passes, (**f**) the second holding time and (**g**) the third holding time. Red arrows in (**c**,**d**) indicate.

3.4. Microstructures

The deformation at 1100 °C led to a microstructure consisting primarily of granular bainitic ferrite (α_B) mixed with a small amount martensite (α') as shown in the OM image of Figure 6a. At this stage of the TMCP simulation, the dynamic ferrite is barely found in the microstructure since only a few ferrite polygonal grains (α_p) of a diameter of approximately 2 to 3 µm were observed. Nevertheless, the addition of deformation passes at 950 °C conducted to significant changes in the material, in all the deformation conditions the specimens exhibited a microstructure that consisted of a mixture of dynamic ferrite and martensite, the former appears in white colour whereas the latter appears dark as shown in Figure 6b–f. The austenite grain refinement caused by the deformation provides more nucleation sites for the dynamic transformation leading to abundant ferrite formation with both morphologies, Widmanstätten ferrite plates (α_w) and polygonal grains. Although the fraction of dynamic ferrite is expected to increase with the deformation, the optical images do not show a significant change in the amount of ferrite in the microstructures as more finishing passes are added. However, a subtle change in the microstructure can be observed after the holding times; ferrite plates exhibit a less sharp aspect and in some

colonies the boundaries between plates commence to disappear (as pointed by the arrow in Figure 6e, and it appears that the amount of polygonal ferrite increases. This change in the microstructure might be given by the continuous coalescence of plates during the holding time.

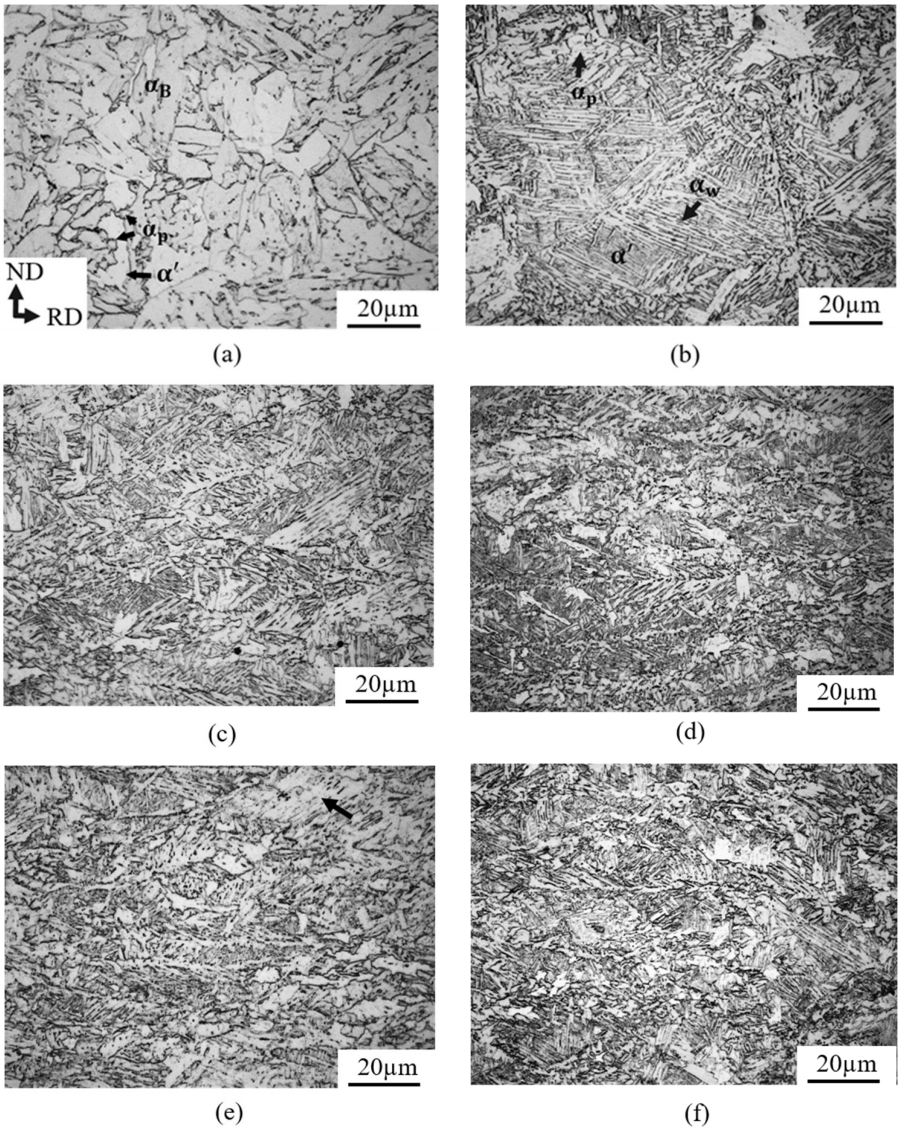

Figure 6. Microstructures revealed in quenched samples after (**a**) rough rolling, (**b**) 1 finishing pass, (**c**) 1 holding time, (**d**) 2 finishing passes, (**e**) 2 holding times and (**f**) 3 holding times.

The coalescence of Widmanstätten ferrite plates and subsequent evolution into polygonal grains can be observed in the SEM images of Figure 7; for which Figure 7a shows a colony of thin plates aligned in a single direction conserving the initial shape resulting from the dynamic transformation (green arrows), as the coalescence process among plates takes place, an intermediate and transitory morphology appears (blue arrows) and then evolve into polygonal grains (red arrows). As the coalescence and polygonisation process continue, the colony of Widmanstätten ferrite plates is practically consumed by the formation of new ultrafine polygonal grains with grain sizes even smaller than 1μm as shown in the Figure 7b.

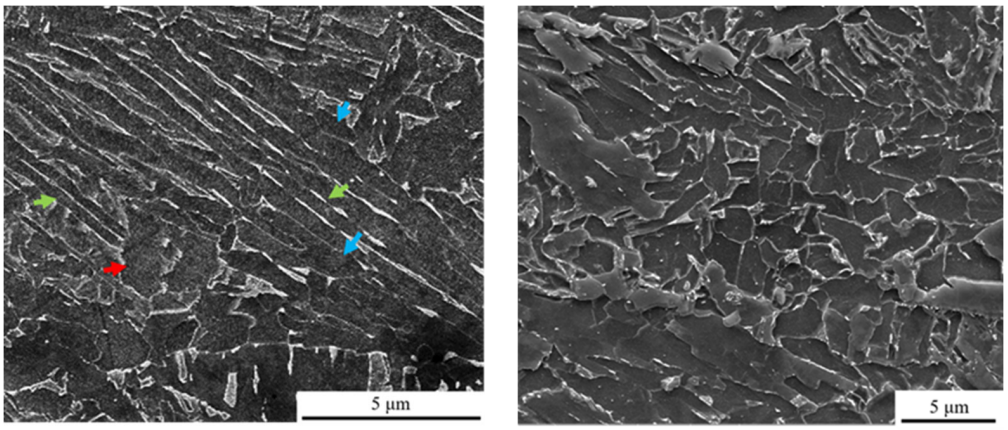

Figure 7. SEM images showing the coalescence of Widmanstätten ferrite plates and subsequent formation of polygonal grains. (**a**) Plates (green arrows) merge leading to the formation of polygonal grains (red arrow), the blue arrows indicate the transitory morphology that takes place during the coalescence of plates prior to the complete polygonisation of grains. (**b**) A colony of fully formed polygonal grains can be observed at the center of the image. The SEM analysis was performed in a quenched specimen obtained after the second holding time at 950 °C.

3.5. EBSD Analysis

Electron back scattered difraction (EBSD) analysis was carried out on a quenched specimen obtained after the second holding time at 950 °C. The crystallographic data was post-processed, and maps were obtained after performing a conservative noise reduction of 7% which increased the index rate to 83%. The criterion for the noise corrections was based on the observation of the distribution of the non-indexed points, the noise was reduced until the main scratches generated during the sample preparation almost disappeared from the EBSD maps. A noise reduction of 7% produced maps with a very good match with the images observed with secondary electrons in SEM. After the noise corrections, most of the non-indexed points were located at features that predictably produce to non-indexed solutions during the EBSD scanning, such as grain and subgrain boundaries, precipitates (all types) and islands of austenite-martensite.

The band slope (BS) technique [34] was used to distinguish between ferrite and martensite in the mixed microstructure. BS is an image quality factor that describes the maximum intensity gradient at the edges of the Kikuchi bands in an EBSD pattern (EBSP), in other words, the BS measures the image quality based on the sharpness of the Kikuchi bands, the higher the BS value, the better the EBSP quality. This technique has been used to separate martensite from ferrite [28,35] due to the great colour contrast produced between both phases, in a grey scale image, martensite appears darker than ferrite because of to the low quality of its EBSP.

A BS map is shown in Figure 8a, in which the ferrite appears as a white colour distributed mainly at the PAGBs, while martensite is found as laths with darker aspect growing within the PAGBs. Note that most of the ferrite appears in form of ultrafine polygonal grains, and the grain and subgrain boundaries are well contoured due to the lower quality of the EBSPs diffracted close to the boundaries. The typical wedge shape of the Widmanstätten ferrite cannot be observed due to the high extent of coalescence of plates, thus polygonal grains are the dominant morphology of ferrite in the microstructure. A most robust evidence of the presence of polygonal ferrite and martensite in the microstructure can be obtained analysing the misorientation angle distribution in each microconstituent. For such purpose, the misorientation was measured in two different regions within the BS map; one region was dominantly ferritic (red dashed square) and the other was dominantly martensitic (yellow dashed oval), both misorientation profiles are plotted in Figure 8b. In the case of polygonal ferrite, the frequency of the angular

misorientation shows that the microstructure possesses a more arbitrary texture, conversely, in martensite the misorientation distribution exhibits a high degree of texturisation, i.e., there is a high frequency only in low and high angle (>50°) boundaries, which is typical from the martensitic transformation [28].

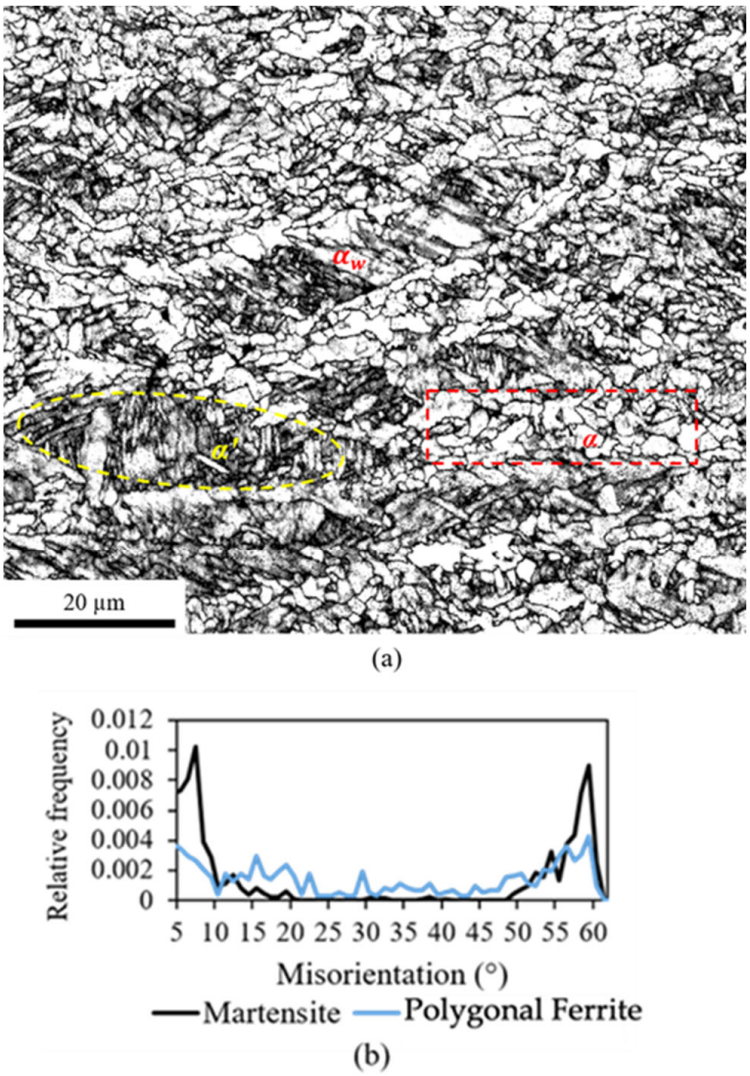

Figure 8. EBSD analysis of the microstructure obtained in the specimen quenched after the second holding time at 950 °C; (**a**) band slope map and (**b**) grain boundaries misorientation distribution of martensite and polygonal ferrite.

3.6. Transmission Electron Microscopy (TEM) Analysis

Figure 9a shows a colony of Widmanstätten ferrite plates undergoing the coalescence process, a fine ferrite plate of about 240 nm wide can be observed at the center of the image, however, most of the plates boundaries cannot be seen due to the removal of dislocations caused by the coalescence. The arrows in this image point out dislocations that form substructures within the ferrite, such substructures are likely to form grain boundaries as the plates merge and evolve into polygonal grains. The subsequent formation of dynamic ferrite grains can be appreciated in Figure 9b, at this stage the plate-like morphology disappeared completely, and some ferrite grains show well defined boundaries (see the arrows).

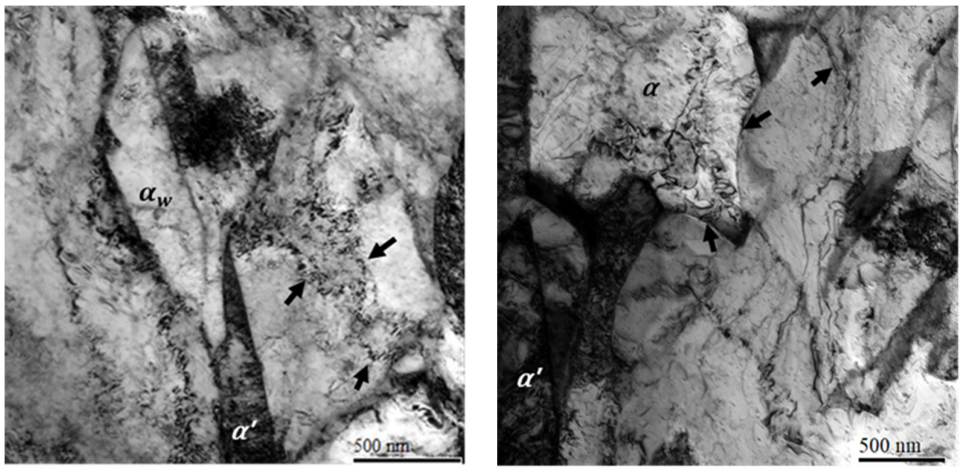

Figure 9. TEM bright field images showing the different morphologies of the dynamic ferrite. (**a**) A colony of Widmanstätten ferrite plates merging, and (**b**) formation of grains. The specimen analysed was quenched after the second finishing pass.

4. Transformation Mechanism and Evolution of Dynamic Ferrite

The results obtained in the current work showed that the dynamic transformation of ferrite follows the path proposed by Basabe et al. [16], which states that the deformation causes the displacive transformation of thin Widmanstätten ferrite plates that then merge by coalescence and evolve into polygonal grains. It was observed that the coalescence process can occur to a large extent statically after the deformation, the analysis of the flow curves demonstrated that significant softening took place during the 10 s of isothermal holding time, particularly during the second holding at 950 °C at which the softening fraction was 71% despite the fact that the recrystallisation of PAGs was negligible. The only plausible explanation for such softening in the material is the evolution of Widmanstätten ferrite colonies into polygonal grains. The microstructures observed in the optical microscope showed that after the holding time of 10 s, the amount of polygonal ferrite increased and the remaining Widmanstätten ferrite colonies lost their typical wedge—shape due to the initiation of the coalescence process.

The evolution path from plates to polygonal grains can be understood by analysing the misorientation of the different morphologies of ferrite in the microstructure. Figure 10a shows a BS-IPF (inverse pole figure) EBSD map made in a region with abundant ferrite (grains and plates). The blue lines in the map represent high angle grain boundaries that have a misorientation equal or greater than 15°, and the brown lines represent low angle grain boundaries or substructures with misorientations from 3 to 15°. The black points are non-indexed pixels which are very likely to be carbides or MA islands as explained before. As reference, a yellow dashed line was drawn manually in the map to indicate the location of a prior austenite grain boundary. The straight lines shown in Figure 10a and represented in Figure 10b–d are misorientation measurements done in ferritic regions with different morphology and location; Figure 10b was drawn within a Widmanstätten ferrite plates colony, Figure 10c along several ultrafine polygonal grains formed intragranulary and Figure 10d is in a wide region of ferrite formed at the PAGB.

In the Widmanstätten ferrite plates colony, the "point to point" profile (Figure 10b) shows that adjacent plates conserve very similar orientation; in a length of 8 μm within a Widmanstätten ferrite colony the misorientation angle does not exceed 2°, this behaviour matches well with the findings reported in other investigations [16,17,36]. However, the point-to-origin profile shows an increase in the misorientation as the distance amongst the plates increases, which is discrepancy with some of those works [17,18,36]. It is important to mention that the misorientation was measured in multiple colonies of Widmanstätten

ferrite using various specimens with different deformation conditions, and in most cases the misorientation showed very similar behaviour.

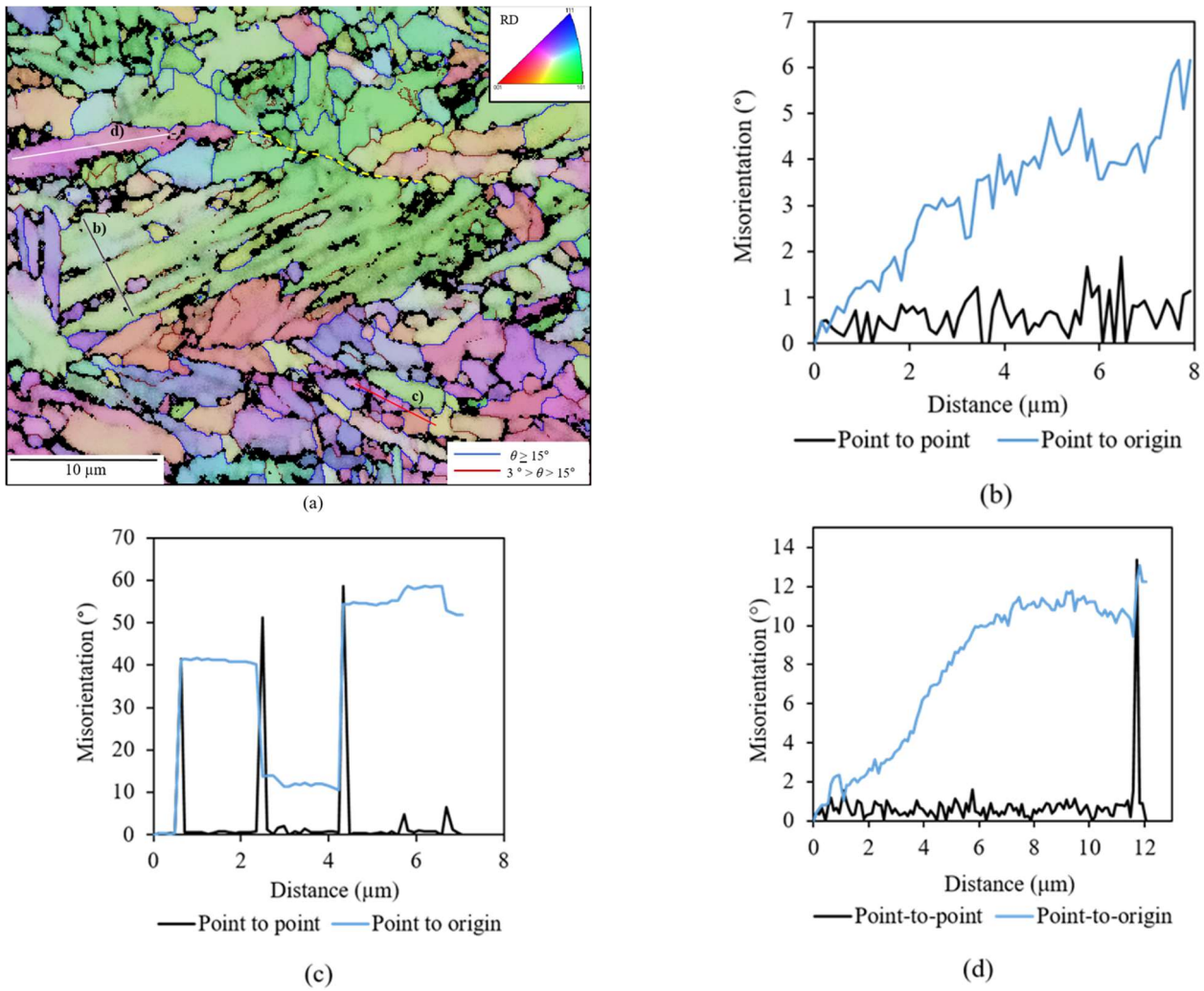

Figure 10. (**a**) Inverse pole figure (IPF) and band contrast EBSD map on the RD-ND plane, the grain boundaries appear in blue colour and subgrains in brown. The three lines in the map are plotted to show the misorientation profile in (**b**) a Widmanstätten ferrite colony, (**c**) a region of ferrite coalescing on the PAGBs and in (**d**) polygonal ferrite grains.

As for the misorientation in the polygonal ferrite (Figure 10c), crystals are highly ordered within the grains which indicates that the coalescence and polygonisation processes already took place leading the formation new grains free of dislocations. The presence of the grain boundaries causes abrupt changes in the orientation from 5 to 59° and the grain diameters range from 1 to 1.9 µm.

Finally, the misorientation in the region of ferrite located at the PAGB (Figure 10d) shows similarities with both, the Widmanstätten ferrite and the ultrafine polygonal ferrite; along approximately the first 8 µm the misorientation has a very similar behaviour to that observed in the colony of Widmanstätten plates, while in the rest of the plot from 8 to 12 µm, the misorientation is more similar to that in the polygonal ferrite. The peak observed in both profiles at around 12 µm, is due to the presence of a grain boundary of a polygonal grain of around 500 nm diameter. Despite having a shape of a single elongated grain located at the PAGBs, the misorientation indicates that such morphology might be instead, the vestiges of a group of ferrite plates coalescing at a stage prior to the complete polygonisation. This finding validates the existence of transitory morphology that occurs

during the coalescence process, in such state the ferrite exhibits characteristics of both displacive and reconstructive transformations.

The coalesce process is a form of recovery that involves the removal or annihilation of dislocations located at the boundaries of the plates, the energy that maintains such process active during the holding time comes from the stored energy of plastic deformation. During the second holding time, the coalescence was the main restoration mechanism operating in the deformed microstructure since the recrystallisation was negligible.

The misorientation observed in the distinct morphologies of ferrite can help understand better the dynamic transformation mechanism of the Widmanstätten ferrite colony. It is suggested that the transformation follows the next steps:

1. The deformation triggers the formation of a pair of self-accommodating ferrite plates following the dynamic transformation mechanism proposed by Jonas & Ghosh [16], the plates conforming the pair of plates possess very similar orientation.
2. A new pair of plates is formed by face-to-face sympathetic nucleation [37] on one of the faces of the pair of plates already formed. This process is repeated in a burst of successive nucleation of pairs of plates. Although adjacent plates have very similar orientation (mainly within the pairs of plates), the continuous nucleation of new pairs of plates widens the ferrite colony leading to a gradual increase in the misorientation with respect to the first pair of plates (the origin).

The transformation mechanism aforementioned describes well the misorientation within the Widmanstätten ferrite colony. The point-to-point profile confirms that the plates have similar orientation between the adjacent faces, whereas the point-to-origin plot, indicates a successive formation of new plates by sympathetic nucleation in which the misorientation increases as more new plates are formed. This formation mechanism explains the intragranular nucleation of plates observed in the present research and that of Basabe et al. [16]. During deformation, the first plates nucleate at the PAGBs, then such plates serve as nucleation sites for new plates leading to intragranular nucleation within the PAGBs.

5. Conclusions

The following conclusions may be drawn from the processing of this high temperature processing (HTP) concept steel.

1. The HTP concept steel showed an excellent microstructural refinement after two finishing passes at 950 °C, a notable austenite conditioning was achieved and the recrystallisation was prevented even after the second holding time of ten seconds. PAGs remained highly elongated in the rolling direction with an average length of 68.4 μm and an aspect ratio of 6.1. Furthermore, a large volume fraction of dynamic ferrite was observed in the microstructure. However, the addition of a third pass followed by a holding time of 10 s led to a large fraction of recrystallisation. Therefore, an adequate design of finish rolling should not include more than two finishing passes at 950 °C (followed by holding times of 10 s) if grain refinement is pursued.
2. The coalescence of plates and polygonisation of grains, are processes that conduct to significant restoration in the deformed microstructure during the 10 s of interpass time in the finish rolling. The analysis of the flow curves showed that after the first interpass time at 950 °C the material experienced a slight hardening of 5%, which indicates a very low work hardening despite the deformation. Then, after the second interpass time the amount of softening resulting in the microstructure was more than 70%, such dramatic softening is directly associated to the evolution of ferrite from plates to grains, since the recrystallisation in this condition was negligible.
3. The behaviour in the internal misorientation in the dynamic ferrite with different morphologies can help unveil the associated transformation mechanism, where it is proposed that dynamic transformation involves the formation of pairs of self-accommodating plates and face to face sympathetic nucleation at the sides of the pairs of plates.

4. During the coalescence of plates prior to the full polygonisation of grains, an intermediate and transitory state of the ferrite appears, in such state the ferrite shares morphological and crystallographic characteristics with both, Widmanstätten ferrite plates and polygonal grains.

Author Contributions: Conceptualization, E.J.P.; Formal analysis, E.P.M.; Investigation, E.P.M.; Writing—review & editing, E.P.M.; Supervision, E.J.P.; Funding acquisition, E.J.P. All authors have read and agreed to the published version of the manuscript.

Funding: This research received no external funding.

Data Availability Statement: The original contributions presented in the study are included in the article, further inquiries can be directed to the corresponding author.

Acknowledgments: The authors would like to thank Companhia Brasileira de Metalurgia e Mineração (CBMM), Brazil for the HTP concept steel used in this investigation. The first author would also like to thank CONACYT (National Council of Science and Technology, Mexico) for financial support.

Conflicts of Interest: The authors declare no conflicts of interest.

References

1. Yada, H.; Matsumura, Y.; Nakahima, K. Ferritic Steel Having Ultra-Fine Grains and a Method for Producing the Same. U.S. Patent 4466842, 21 August 1984.
2. Yada, H.; Matsumura, Y.; Senuma, T. Massive type transformation induced by hot deformation in low carbon steels, in Proceedings of the international conference on martensitic transformation. *Jpn. Inst. Mater.* **1986**, 515–520.
3. Yada, H.; Matsumura, Y.; Senuma, T. A new thermomechanical heat treatment for grain refining in low carbon steels. In Proceedings of the 1st Conference on Physical Metallurgy of Thermomechanical Processing of Steels and Other Metals, ISIJ 1988, THERMEC-88, Tokyo, Japan, 6–10 June 1988; Tamura, I.I., Ed.; pp. 200–207.
4. Gong, P.; Sun, L.; Wynne, B.P.; Palmiere, E.J.; Rainforth, W.M. The effect of thermomechanical controlled processing on recrystallisation and subsequent deformation-induced ferrite transformation textures in microalloyed steels. *J. Mater. Sci.* **2018**, *53*, 6922–6938. [CrossRef]
5. Ferreira, J.C.; Machado, F.R.S.; Aranas, C.; Siciliano, F.; Reis, G.S.; de Miranda, E.J.P.; Paiva, A.E.M.; Rodrigues, S.F. Physical simulation based on dynamic transformation under hot plate rolling of a Nb-microalloyed steel. *Front. Mater.* **2021**, *8*, 716967. [CrossRef]
6. Eres-Castellanos, A.; Garcia-Mateo, C.; Caballero, F.G. Future trends on displacive stress and strain induced transformations in steels. *Metals* **2021**, *11*, 299. [CrossRef]
7. Monschein, S.; Ragger, K.S.; Fasching, J.; Zügner, D.; Schnitzer, R. Microstructural, chemical, and crystallographic investigations of dynamic strain-induced ferrite in a microalloyed QT steel. *Metals* **2022**, *12*, 313. [CrossRef]
8. Li, H.; Zheng, X.; Fan, L.; Xu, H.; Tian, Y.; Dai, X.; Chen, L. Ultrafine grain ferrite transformed from fine austenite grains produced by dynamic reversal transformation. *Materials* **2022**, *15*, 8727. [CrossRef] [PubMed]
9. Yada, H.; Li, C.M.; Yamagata, H. Dynamic $\gamma \rightarrow \alpha$ transformation during hot deformation in iron-nickel-carbon alloys. *ISIJ Int.* **2000**, *40*, 200–206. [CrossRef]
10. Liu, Q.Y.; Deng, S.H.; Sun, X.J.; Dong, H.; Weng, Y.Q. Effect of dissolved and precipitated niobium in microalloyed steel on deformation induced ferrite transformation (DIFT). *J. Iron Steel Res. Int.* **2009**, *16*, 67–71. [CrossRef]
11. Hodgson, P.D.; Beladi, H. Dynamic strain-induced ferrite transformation (DSIT) in steels. In *Phase Transformations in Steels. Volume 1: Fundamentals and Diffusion Controlled Transformations*; Pereloma, E., Edmonds, D.V., Eds.; Woodhead Publishing in Materials: Cambridge, UK, 2012; Volume 1, pp. 527–554.
12. Dong, H.; Sun, X.J. Deformation induced ferrite transformation in low carbon steels. *Curr. Opin. Solid State Mater. Sci.* **2005**, *9*, 269–276. [CrossRef]
13. Sun, L.; Muszka, K.; Wynne, B.P.; Palmiere, E.J. Effect of strain path on dynamic strain-induced transformation in a microalloyed steel. *Acta Mater.* **2014**, *66*, 132–149. [CrossRef]
14. Gong, P.; Palmiere, E.J.; Rainforth, W.M. Thermomechanical processing route to achieve ultrafine grains in low carbon microalloyed steels. *Acta Mater.* **2016**, *119*, 43–54. [CrossRef]
15. Carneiro, T.B.; Rodrigues, S.F.; Aranas, C.; Siociliano, F.; Silva, E.S.; Reis, G.S.; Miranda, E.J.P.; Leal, G.S.; Jahazi, M.; Jonas, J.J. Retransformation of dynamically induced ferrite during physical simulation of Steckel mill hot rolling. *J. Mater. Res. Technol.* **2020**, *9*, 10254–10264. [CrossRef]
16. Basabe, V.V.; Jonas, J.J.; Ghosh, C. Formation of Widmanstatten ferrite in a 0.036% Nb low carbon steel at temperatures above the Ae_3. *Steel Res. Int.* **2014**, *85*, 8–15. [CrossRef]
17. Ghosh, C.; Basabe, V.V.; Jonas, J.J.; Yue, S.; Xiong, X.Y. Dynamic transformation behavior of a deformed high carbon steel at temperatures above the Ae_3. *ISIJ Int.* **2013**, *53*, 900–908. [CrossRef]

18. Ghosh, C.; Basabe, V.V.; Jonas, J.J.; Kim, Y.M.; Jung, I.H.; Yue, S. The dynamic transformation of deformed austenite at temperatures above the Ae_3. *Acta Mater.* **2013**, *61*, 2348–2362. [CrossRef]
19. Ghosh, C.; Basabe, V.V.; Jonas, J.J. Thermodynamics of dynamic transformation of hot deformed austenite in four steels of increasing carbon contents. *Mater. Sci. Eng. A* **2014**, *591*, 173–182. [CrossRef]
20. Grewal, R.; Aranas, C.; Chadha, K.; Shahriari, D.; Jahazi, M.; Jonas, J.J. Formation of Widmanstatten ferrite at very high temperatures in the austenite phase field. *Acta Mater.* **2016**, *109*, 23–31. [CrossRef]
21. Rodrigues, S.F.; Aranas, C.; Jonas, J.J. Dynamic transformation during the simulated plate rolling of a 0.09% Nb steel. *ISIJ Int.* **2017**, *57*, 1102–1111. [CrossRef]
22. Jonas, J.J.; Ghosh, C. Role of mechanical activation in the dynamic transformation of austenite. *Acta Mater.* **2013**, *61*, 6125–6131. [CrossRef]
23. Jonas, J.J.; He, Y.; Langelaan, G. The rotation axes and angles involved in the formation of self-accommodating plates of Widmanstatten ferrite. *Acta Mater.* **2014**, *72*, 13–21. [CrossRef]
24. Loveday, M.S.; Mahon, G.J.; Roebuck, B.; Lacey, A.J.; Palmiere, E.J.; Sellars, C.M.; Van Der Winden, M.R. Measurement of flow stress in hot plane strain compression tests. *Mater. High Temp.* **2006**, *23*, 85–118. [CrossRef]
25. Thackray, R.; Palmiere, E.J.; Khalid, O. Novel etching technique for delineation of prior-austenite grain boundaries in low, medium and high carbon steels. *Materials* **2020**, *13*, 3296. [CrossRef] [PubMed]
26. Rodriguez-Galeano, K.F.; Romano-Acosta, L.F.; Palmiere, E.J.; Rainforth, W.M. A new approach to etching low-carbon microalloyed steels to reveal prior austenite grain boundaries and the dual-phase microstructure. *J. Microsc.* **2023**, *289*, 73–79. [CrossRef] [PubMed]
27. Collins, J.; Taylor, M.; Scarlett, A.L.; Palmiere, E.J.; Pickering, E.J. Prior austenite grain measurement: A direct comparison of EBSD reconstruction, thermal etching and chemical etching. *Mater. Charact.* **2024**, *208*, 113656. [CrossRef]
28. Ryde, L. Application of EBSD to analysis of microstructures in commercial steels. *Mater. Sci. Technol.* **2006**, *22*, 1297–1306. [CrossRef]
29. Zhu, K.; Bouaziz, O.; Oberbillig, C.; Huang, M. An approach to define the effective lath size controlling yield strength of bainite. *Mater. Sci. Eng. A* **2010**, *527*, 6614–6619. [CrossRef]
30. Kwon, O.; DeArdo, A.J. On the recovery and recrystallization which attend static softening in hot-deformed copper and aluminum. *Acta Metall. Mater.* **1990**, *38*, 41–54. [CrossRef]
31. Romano-Acosta, L.F.; Garcia-Rincon, O.; Pedraza, J.P.; Palmiere, E.J. Influence of thermomechanical processing parameters on critical temperatures to develop an advanced high-strength steel microstructure. *J. Mater. Sci.* **2021**, *56*, 18710–18721. [CrossRef]
32. Mendes-Fonseca, N.; Rodrigues, S.F.; Guo, B.; Jonas, J.J. Dynamic transformation during the simulated hot rolling of an API-X80 steel. *Steel Res. Int.* **2019**, *90*, 1900091. [CrossRef]
33. Palhano, H.B.; Aranas, C.; Rodrigues, S.F.; Silva, E.S.; Reis, G.S.; Miranda, E.J.P.; Siciliano, F.; Jonas, J.J. Strain-induced ferrite formation during Steckel mill simulations with varying roughing pass schedules. *Metals* **2019**, *9*, 814. [CrossRef]
34. Day, A.; Trimby, P. *Channel 5 Manual*; HKL Technology: Hobro, Denmark, 2001.
35. Kang, J.Y.; Park, S.J.; Moon, M.B. Phase analysis on dual-phase steel using band slope of electron backscatter diffraction pattern. *Microsc. Microanal.* **2013**, *19*, 13–16. [CrossRef]
36. Basabe, V.V.; Jonas, J.J.; Ghosh, C. Formation of strain-induced ferrite in low carbon steels at temperatures above the Ae_3. *ISIJ Int.* **2013**, *53*, 2233–2241. [CrossRef]
37. Aaronson, H.I.; Spanos, G.; Masamura, R.A.; Vardiman, R.G.; Moon, D.W.; Menon, E.S.K.; Hall, M.G. Sympathetic nucleation-an overview. *Mater. Sci. Eng. B* **1995**, *32*, 107–123. [CrossRef]